Applications and Applied Mathematics: An International Journal (AAM)

Volume 16 | Issue 2 Article 11

12-2021

(R1464) Stability of the Artificial Equilibrium Points in the Low-Thrust Restricted Three-Body Problem with Variable Mass

Amit Mittal
University of Delhi

Krishan Pal
University of Delhi

Pravata Kumar Behera
University of Delhi

Deepak Mittal
University of Delhi

Available at
http://pvamu.edu/aam
Appl. Appl. Math.
ISSN: 1932-9466

Applications and Applied Mathematics:
An International Journal
(AAM)

Vol. 16, Issue 2 (December 2021), pp. 965 – 989

Stability of the Artificial Equilibrium Points in the Low-Thrust Restricted Three-Body Problem with Variable Mass

[1]Amit Mittal, [2*]Krishan Pal, [3]Pravata Kumar Behera, and [4]Deepak Mittal

[1,3] Department of Mathematics & Physics
A.R.S.D College
University of Delhi, India
[1]to.amitmittal@gmail.com
[3]pravat.arsd@gmail.com

[2*] Department of Mathematics
Maharaja Agrasen College
University of Delhi, India
kpal1987@gmail.com

[4] Department of Computer Science
Deen Dayal Upadhaya College
University of Delhi, India
to.deepaktmittal@gmail.com

Received: December 12, 2020; Accepted: February 24, 2021

Abstract

In this article, we have investigated the existence and stability of the artificial equilibrium points (AEPs) in the low-thrust restricted three-body problem with variable mass. In this model of the low-thrust restricted three-body problem, we have considered both the primaries as point masses. The mass of the spacecraft varies with time according to Jeans' law (1928). We have introduced a new concept for creating the AEPs in the restricted three-body problem with variable mass using continuous constant acceleration. We have derived the equations of motion of the spacecraft after using the space-time transformations of Meshcherskii. The AEPs have been created by cancelling the gravitational and centrifugal forces with the constant continuous low-thrust at the non-equilibrium points. The positions of these AEPs will depend not only on magnitude but also on the constant directions of the low-thrust acceleration. We have analyzed the linear stability of the AEPs and found that all the AEPs are unstable. Finally, we have drawn the zero velocity curves (ZVCs) to determine the possible regions of motion in which the spacecraft is free to move.

Keywords: Restricted three-body problem; Artificial equilibrium point; Zero velocity curves; Stability; Low-thrust; Variable mass

MSC 2010 No.: 37N0, 70F07, 70F15

1. Introduction

In celestial mechanics, the new idea of research on variable mass in the two body problem has been introduced by Jeans (1928) to study the motion of a binary system. In the new corporated study, he has investigated the equations of motion of two body problem with variable mass. After Jeans' work on variable mass, Meshcherskii (1949,1952) has introduced the same idea on variable mass in the two body problem with some other perturbations. He believed that mass is ejected isotropically from the included system of two bodies with high velocities and is lost to the system. In his study, he has determined the change in orbits, the variation in angular momentum and the energy of the system.

The restricted three-body problem has been formulated by Szebehely (1967). After the idea on variable mass, in a series of papers, Shrivastava and Ishwar (1983) and Sing and Ishwar (1984, 1985) have studied the restricted three-body problem under the assumption that the mass of the infinitesimal body is decreasing with time. Also, the latest concept of variable mass was applied by Lu (1990) in his research work. He has investigated the stability of triangular equilibrium points in the restricted problem of three-bodies with variable mass. Many perturbing forces such as radiation, oblateness, and variation of mass have been studied by many scientists and authors. The non-linear stability of the triangular equilibrium points in the R3BP (see Singh (2008), (2009), (2011)), the linear stability of the equilibrium points in the photo-gravitational R3BP (see Singh (2003), Singh and Leke (2010), Zhang et al. (2012)), the existence of out-of-plane equilibrium points in the R3BP (see Abouelmagd and Mostafa (2015)).

In addition, Mittal et al. (2016, 2018a) have investigated the stability of the Lagrangian solutions for the restricted four-body problem with variable mass. Also, Mittal et al. (2018b) have investigated the basins of convergence in the planar circular restricted four-body problem with variable mass. Recently, Suraj et al. (2018a, 2018b) have investigated the restricted four-body problem with variable mass. Further, Suraj et al. (2019) have studied the restricted five-body problem with variable mass. Moreover, Suraj et al. (2020a) have incorporated Copenhagen problem with a repulsive quasi-homogeneous Manev-type potential with variable mass. In their study, they have discussed the stability of in-plane and out-of-plane equilibrium points. Also, Suraj et al. (2018a, 2018b, 2019, 2020a) have studied the basins of convergence associated with the libration points in the restricted three-body, four-body and five-body problems.

The low-thrust restricted three-body problem is one of the important problem in the field of celestial mechanics for establishing the artificial satellites in the regions of space. The new equilibrium points can be obtained if the continuous low-thrust is used by a spacecraft to balance the gravitational and centrifugal forces at the non-equilibrium points. These points are usually referred to Artificial Equilibrium Points (AEPs). Farquhar (1967) has studied the concept of telecommunication systems using Lagrange points and investigated ballistic periodic orbits about these points in the Earth-Moon system. Further, Dusek (1966) and Broschart and Scheeres (2005) have studied the stability of equilibrium points with continuous control acceleration. The similar research in the low-thrust restricted three-body problem is focussed by many authors. In the beginning, the low-thrust R3BP with different versions has been studied by many authors such as Morimoto et al. (2007), Baig and McInnes (2008), Bombardelli and Pelaez (2011), Aliasi et al. (2011), Ranjana and Kumar (2013),

and Yang et al. (2015) studied the AEPs and their stability. Aliasi et al. (2012) studied the AEPs and their stability in the elliptic restricted three-body problem with solar-sail.

Further, Bu et al. (2017) have investigated the positions and dynamical characteristic of AEPs in a binary asteroid system with continuous low-thrust. Furthermore, Mittal and Pal (2018) have studied the existence and stability conditions of the AEPs in the circular restricted three-body problem when both the primaries are oblate spheroids. More, recently Suraj et al.(2020b, 2020c) have investigated the existence and stability of the AEPs in the circular restricted three-body problem under the influences of radiation pressure and oblateness, respectively.

In this article, we have studied the existence and linear stability of AEPs in the low-thrust restricted three-body problem with variable mass when both the primaries as point masses. This paper has been discussed in few sections. In Section 1, we have introduced our problem. In Section 2, we have derived the equations of motion of the spacecraft. In Section 3, we have found the locations of the AEPs. In Section 4, we have analyzed the linear stability of the AEPs. In Section 5, we have discussed the zero velocity curves. In Section 6, we have discussed our problem and the results obtained. Finally, in Section 7, we have concluded the results obtained.

2. Equations of Motion

In this section, we consider a model of low-thrust restricted three-body problem with variable mass. Here, we have discussed the motion of an infinitesimal (spacecraft) body of mass m which is moving under the influence of two primary bodies of masses m_1 and m_2 $(m_1 \geq m_2)$. There are two forces acting on the infinitesimal body of mass m. First, one is combined gravitational attractions of the primaries, and the second one is continuous low-thrust acceleration working along the x, y and z axes. The directions of components $(a_x,\, a_y,\, a_z)$ of continuous low-thrust acceleration are displayed in the configuration of the problem (see Figure 1). Let the primaries be revolving with angular velocity ω in circular orbits about their common center of mass O considered as origin. Let the infinitesimal body (spacecraft) of mass m be moving in the plane of motion of m_1 and m_2. The motion of the spacecraft is influenced by the motion of m_1 and m_2 but not affects them.

In this problem, we assume that both the primaries are point masses. The line joining the primaries m_1 and m_2 is taken as x-axis and the line passes through O and perpendicular to the x-axis and lying in the plane of motion of m_1 and m_2 is considered as y-axis. The line which passes through the origin and perpendicular to the plane of motion of the primaries is taken as z-axis. We have considered the synodic coordinate system $O\,(xyz)$, initially coincident with the inertial coordinate system $O\,(XYZ)$, rotating with the angular velocity ω about z-axis (the z-axis is coincident with the Z-axis). Let us consider the primaries of masses m_1 and m_2 be located at $(-\mu,\, 0,\, 0)$ and $(1-\mu,\, 0,\, 0)$, respectively, and the spacecraft is located at the point $(x,\, y,\, z)$ (see Figure 1). We scale the units by taking the sum of the masses and the distance between the primaries both equal to unity. Therefore, $m_1 = 1-\mu$, $m_2 = \mu$, $\mu = \frac{m_2}{m_1+m_2}$ and $\mu \in (0,\, 0.5]$ with $m_1 + m_2 = 1$. Also, we have chosen the units of time so that the gravitational constant $G = 1$ and the angular velocity $\omega = 1$. We shall determine the equations of motion of the spacecraft with variable mass by adopting

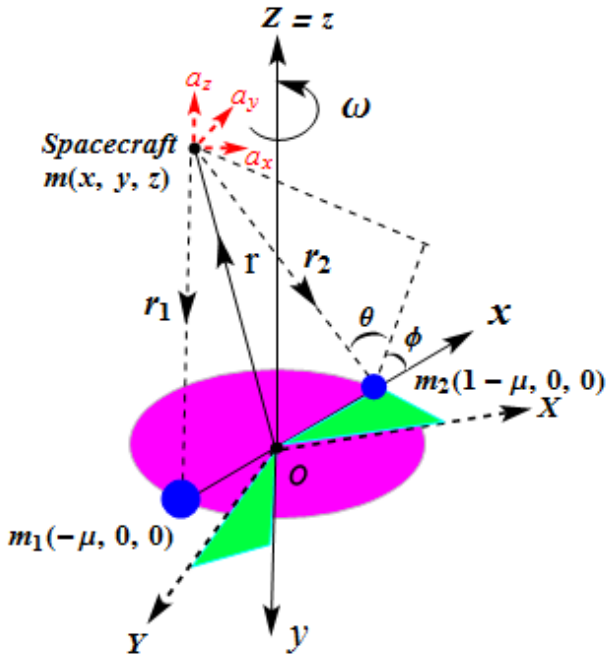

Figure 1. Configuration of the problem

the procedure of Mittal et al. (2016). Thus, the equations of motion of the spacecraft with continuous low-thrust in dimensionless co-ordinate system can be written as:

$$\left.\begin{aligned} \dot{m}\,(\dot{x}-y)+m\,(\ddot{x}-2\dot{y}) &= -U_x+a_x,\\ \dot{m}\,(\dot{y}+x)+m\,(\ddot{y}+2\dot{x}) &= -U_y+a_y,\\ \dot{m}\,\ddot{z} &= -U_z+a_z. \end{aligned}\right\} \tag{1}$$

The continuous low-thrust acceleration in the rotating coordinate system is given by $\boldsymbol{a} = (a_x,\, a_y,\, a_z)^{\,T}$. The components along the three axes are:

$$\left.\begin{aligned} a_x &= a\,\cos\,\theta\,\cos\,\phi,\\ a_y &= a\,\cos\,\theta\,\sin\,\phi,\\ a_z &= a\,\sin\,\theta, \end{aligned}\right\}$$

where a is dimensionless magnitude of continuous control acceleration $\boldsymbol{a}$, θ and ϕ are the direction angles of continuous control acceleration $\boldsymbol{a}$. The direction angles are shown in the configuration of the problem in Figure 1. θ is the angle between the direction of control and the xy-plane, ϕ is the angle between the direction of control and the direction of the x-axis, and U is the potential of the system without continuous low-thrust and given by

$$U = -\frac{m}{2}(x^2+y^2) - m\left(\frac{1-\mu}{r_1}+\frac{\mu}{r_2}\right),$$

$$r_1 = \sqrt{(x+\mu)^2+y^2+z^2},$$

$$r_2 = \sqrt{(x+\mu-1)^2 + y^2 + z^2}.$$

Let us consider the mass of the spacecraft varies with time t according to Jeans' law (1928)

$$\frac{dm}{dt} = -\alpha m^n, \tag{2}$$

where α is constant coefficient and the value of exponent n is within the limit $0.4 \leq n \leq 4.4$ (for the star of main sequence). For a rocket, $n = 1$ and the mass of the rocket varies exponentially and given by the expression $m = m_0\, e^{-\alpha t}$, where m_0 is mass of the spacecraft at time $t = 0$. We simplify the equations of motion by using the space time transformations

$$\xi = \gamma^q\, x, \eta = \gamma^q\, y, \zeta = \gamma^q\, z, d\Gamma = \gamma^k dt, r_1 = \gamma^{-q}\, \rho_1, r_2 = \gamma^{-q}\, \rho_2, \tag{3}$$

where $\gamma = \frac{m}{m_0}$.

Considering the procedure of Mittal et al. (2016) by taking $q = \frac{1}{2}, k = 0, n = 1$ and using equations (2) and (3), the equations (1) can be transformed into the equations:

$$\left.\begin{aligned} \ddot{\xi} - 2\dot{\eta} &= -\Omega_\xi + \frac{1}{\sqrt{\gamma}}\, a\, \cos\,\theta\, \cos\,\phi = -\Omega^*_\xi, \\ \ddot{\eta} + 2\dot{\xi} &= -\Omega_\eta + \frac{1}{\sqrt{\gamma}}\, a\, \cos\,\theta\, \sin\,\phi = -\Omega^*_\eta, \\ \ddot{\zeta} &= -\Omega_\zeta + \frac{1}{\sqrt{\gamma}}\, a\, \sin\,\theta = -\Omega^*_\zeta. \end{aligned}\right\} \tag{4}$$

The above system of differential equations are the equations of motion of the spacecraft with variable mass, which are different from the equations of motion of constant mass. The effective potential function of the system without continuous low-thrust is defined as

$$\Omega = -\frac{1}{2}\left(1 + \frac{\alpha^2}{4}\right)(\xi^2 + \eta^2) - \gamma^{3/2}\left(\frac{1-\mu}{\rho_1} + \frac{\mu}{\rho_2}\right) - \frac{\alpha^2}{8}\zeta^2.$$

Thus, the effective potential function of the system with continuous low-thrust is given by:

$$\Omega^* = -\frac{1}{2}\left(1 + \frac{\alpha^2}{4}\right)(\xi^2 + \eta^2) - \gamma^{3/2}\left(\frac{1-\mu}{\rho_1} + \frac{\mu}{\rho_2}\right) - \frac{\alpha^2}{8}\zeta^2 - \frac{1}{\sqrt{\gamma}}\,(a_\xi\,\xi + a_\eta\,\eta + a_\zeta\,\zeta),$$

where $\rho_1 = \sqrt{(\xi-\xi_1)^2 + \eta^2 + \zeta^2}$, $\rho_2 = \sqrt{(\xi-\xi_2)^2 + \eta^2 + \zeta^2}$, $\xi_1 = -\mu\gamma^{1/2}$, $\xi_2 = (1-\mu)\,\gamma^{1/2}$, and

$$\left.\begin{aligned} a_\xi &= a\, \cos\,\theta\, \cos\,\phi, \\ a_\eta &= a\, \cos\,\theta\, \sin\,\phi, \\ a_\zeta &= a\, \sin\,\theta. \end{aligned}\right\}$$

The magnitude of control acceleration is given as $a = \sqrt{a_\xi^2 + a_\eta^2 + a_\zeta^2}$. From Equations (4), we have obtained

$$\dot{\xi}^2 + \dot{\eta}^2 + \dot{\zeta}^2 = -\left(2\Omega^* - C - 2\int_0^t \Omega_t^* dt\right), \tag{5}$$

where C is Jacobian constant.

3. Locations of the artificial equilibrium points

We can find the artificial equilibrium points (AEPs) from the solutions of the equations $\Omega_\xi^* = 0$, $\Omega_\eta^* = 0$, $\Omega_\zeta^* = 0$, i.e.,

$$\left.\begin{aligned}\left(1+\frac{\alpha^2}{4}\right)\xi_0 - \gamma^{3/2}\frac{(1-\mu)(\xi_0+\mu\sqrt{\gamma})}{\rho_1^3} - \gamma^{3/2}\frac{\mu(\xi_0+(-1+\mu)\sqrt{\gamma})}{\rho_2^3} \\ +\frac{1}{\sqrt{\gamma}}a\cos\theta\cos\phi = 0, \\ \left(1+\frac{\alpha^2}{4}\right)\eta_0 - \gamma^{3/2}\frac{(1-\mu)\eta_0}{\rho_1^3} - \gamma^{3/2}\frac{\mu\eta_0}{\rho_2^3} + \frac{1}{\sqrt{\gamma}}a\cos\theta\sin\phi = 0, \\ \frac{\alpha^2}{4}\zeta_0 - \gamma^{3/2}\frac{(1-\mu)\zeta_0}{\rho_1^3} - \gamma^{3/2}\frac{\mu\zeta_0}{\rho_2^3} + \frac{1}{\sqrt{\gamma}}a\sin\theta = 0\,.\end{aligned}\right\} \tag{6}$$

We have obtained the control acceleration components $(a_\xi,\, a_\eta,\, a_\zeta)$ for an AEP $(\xi_0,\, \eta_0,\, \zeta_0)$ as:

$$\left.\begin{aligned}a_\xi = -\sqrt{\gamma}\left(1+\frac{\alpha^2}{4}\right)\xi_0 + \gamma^2\frac{(1-\mu)(\xi_0+\mu\sqrt{\gamma})}{\rho_1^3} + \gamma^2\frac{\mu(\xi_0+(-1+\mu)\sqrt{\gamma})}{\rho_2^3}, \\ a_\eta = -\sqrt{\gamma}\left(1+\frac{\alpha^2}{4}\right)\eta_0 + \gamma^2\frac{(1-\mu)\eta_0}{\rho_1^3} + \gamma^2\frac{\mu\eta_0}{\rho_2^3}, \\ a_\zeta = -\sqrt{\gamma}\,\frac{\alpha^2}{4}\zeta_0 + \gamma^2\frac{(1-\mu)\zeta_0}{\rho_1^3} + \gamma^2\frac{\mu\zeta_0}{\rho_2^3}.\end{aligned}\right\} \tag{7}$$

3.1. The AEPs for $\theta = 0$, $\phi \in [0, 2\pi]$

If $\theta = 0$ and $\phi \in [0, 2\pi]$, we have obtained $\zeta = 0$, therefore, the AEPs are lying in the $\xi\eta$-plane and obtained from Equestions (6) by taking $\zeta = 0$. The collinear AEPs are the roots of the equation

$$\begin{aligned}g(\xi,\, 0,\, 0) = &-\left(1+\frac{\alpha^2}{4}\right)\xi_0 + \gamma^{3/2}\frac{(1-\mu)(\xi_0+\mu\sqrt{\gamma})}{\rho_1^3} \\ &+\gamma^{3/2}\frac{\mu(\xi_0+(-1+\mu)\sqrt{\gamma})}{\rho_2^3} - \frac{1}{\sqrt{\gamma}}a\cos\theta\cos\phi = 0\,.\end{aligned}$$

The non-collinear AEPs are lying in the $\xi\,\eta$-plane but not on ζ-axis. The non-collinear AEPs are obtained from Equestions (6) by taking $\xi \neq 0$, $\eta \neq 0$, $\zeta = 0$ and $\theta = 0$, $\phi = \pi/2$. The positions of these AEPs will depend not only on magnitude but also on the directions of continuous low-thrust

acceleration $\boldsymbol{a}$. If we take $\alpha = 0$ (or $\gamma = 1$) and $a = 0$, then the above Equestions (6) reduce to the equations obtained by Szebehely (1967). When $\alpha = 0$ (or $\gamma = 1$) and $a \neq 0$, then above Equestions (6) reduce to the equations obtained by Morimoto et al. (2007). Solving Equestions (6) for $\zeta = 0$, then AEPs are the solutions of $\Omega^*_\xi = 0$ and $\Omega^*_\eta = 0$. We have obtained the five AEPs denoted by L_1, L_2, L_3, L_4 and L_5 for the given parameters. In Tables $1, 2, 3,$ and 4, we have displayed the numerical values of these AEPs for fixed values of $\mu = 0.019$, $\gamma = 0.1$ and different values of a, θ, ϕ and α. From Tables 1 and 3, it is observed that there exist three collinear and two non-collinear AEPs if the direction of acceleration is going to the positive ξ-axis. Further, from Tables 2 and 4, it is noticed that there exist only five non-collinear AEPs when the direction of acceleration is going to the positive η-axis.

The locations of the AEPs with variable mass are shown in Figure (2) and Figure (3) for fixed values of $\mu = 0.019$, $\gamma = 0.1$ and for different values θ, ϕ, a and α. In Figure (2) we have plotted the AEPs for $\mu = 0.019$, $\alpha = 0.2$, $\gamma = 0.1$, (a) for $\theta = 0$, $\phi = 0$ and $a = 0.00015\,(gray,\, red)$, $0.00035\,(gray,\, green)$, $0.00055\,(gray,\, magenta)$, $0.00075\,(gray,\, orange)$, (b) for $\theta = 0$, $\phi = \pi/2$ and $a = 0.00015\,(gray,\, red)$, $0.00035\,(gray,\, green)$, $0.00055\,(gray,\, magenta)$, and $0.00075\,(gray,\, orange)$. From Figure 2(a), we have observed that when the magnitude a is increasing, the movements of AEPs L_1, L_2 and L_3 are almost negligible, and L_4 and L_5 move towards the η-axis. It is observed that the AEPs L_4 and L_5 are symmetric about the ξ-axis. From Figure 2, panel (b), we have observed that when the magnitude a is increasing, the AEPs L_1, L_2 and L_3 move away from the primaries m_1 and m_2. The AEP L_4 moves towards the primary m_2 while the AEP L_5 moves away from it. Also, in this case, it is found that the AEPs L_4 and L_5 are not symmetric about the ξ-axis.

In Figure 3, we have plotted the AEPs for $\mu = 0.019$, $\gamma = 0.1$, (a) for $\theta = 0$, $\phi = 0$, $a = 0.0015$ and $\alpha = 0.2\,(gray,\, red)$, $0.4\,(gray,\, green)$, $0.6\,(gray,\, magenta)$, $0.8\,(gray,\, orange)$, $1\,(gray,\, cyan)$, (b) is the zoomed part of panel (a) near the primary m_2, (c) for $\theta = 0$, $\phi = \pi/2$, $a = 0.0015$ and $\alpha = 0.2\,(gray,\, red)$, $0.4\,(gray,\, green)$, $0.6\,(gray,\, magenta)$, $0.8\,(gray,\, orange)$, $1\,(gray,\, cyan)$. From Figure 3, panel (a), we have observed that when α is increasing, the AEP L_1 is shifted from right to left towards the primary m_1 and the AEP L_2 is also shifted from right to left towards the primary m_2. The AEP L_3 is shifted from left to right towards the bigger primary m_1 and L_4 and L_5 move towards the ξ-axis. Further, we have found that the AEPs L_4 and L_5 are symmetric about the ξ-axis.

From Figure 3(c), we have observed that when α is increasing, the AEP L_1 is shifted from right to left towards the primary m_1 and the AEP L_2 is also shifted from right to left towards the primary m_2 and the AEPs L_3, L_4 and L_5 move towards the ξ-axis. In addition, we have found that the AEPs L_4 and L_5 are not symmetric with respect to ξ-axis. We have also observed that the AEPs with variable mass are the new positions of the equilibrium points under the effect of continuous low-thrust and the parameters α and γ, these positions are different from the natural equilibrium points.

3.2. The AEPs for $\phi = 0, \theta \in [0, 2\pi]$

When $\phi = 0$ and $\theta \in [0, 2\pi]$, we have obtained $\eta = 0$, therefore, the AEPs are lying in the $\xi\zeta$-plane and obtained from Equestions (6) by taking $\eta = 0$. The AEPs which lie in $\xi\zeta$-plane ($\eta = 0$) are called out-of-plane AEPs. In Figure 4, we have displayed the positions of the out-of-plane AEPs denoted by L_6 and L_7. The out-of-plane AEPs are calculated from Equestions (6) by taking $\xi \neq 0, \zeta \neq 0$ and $\eta = 0$. We have plotted the out-of-plane AEPs for $\mu = 0.019$, $\alpha = 0.2$, $\gamma = 0.1$ (a) $\theta = 0$, $\phi = 0$ and $a = 0.0015\,(gray,\ red)$, $0.0035\,(gray,\ green)$, $0.0055\,(gray,\ magenta)$, $0.0075\,(gray,\ orange)$ and $0.0095\,(gray,\ cyan)$, (b) $\theta = \pi/2$, $\phi = 0$ and $a = 0.0015\,(gray,\ red)$, $0.0035\,(gray,\ green)$, $0.0055\,(gray,\ magenta)$, $0.0075\,(gray,\ orange)$, $0.0095\,(gray,\ cyan)$ and $\alpha = 0.2$, (c) for $\theta = 0$, $\phi = 0$, $a = 0.00015$ and $\alpha = 0.2\,(gray,\ red)$, $0.4\,(gray,\ green)$, $0.6\,(gray,\ magenta)$, $0.8\,(gray,\ orange)$, $1\,(gray,\ cyan)$, (d) for $\theta = \pi/2$, $\phi = 0$, $a = 0.00015$ and $\alpha = 0.2\,(gray,\ red)$, $0.4\,(gray,\ green)$, $0.6\,(gray,\ magenta)$, $0.8\,(gray,\ orange)$, $1\,(gray,\ cyan)$.

From Figure 4, panel (a), we have observed that when the magnitude a is increasing, the AEPs $L_{6,7}$ move towards the ζ-axis and away from the primaries. Also, we have found the AEPs $L_{6,7}$ which are symmetrical about the ξ-axis. From Figure 4, panel (b), we have observed that when the magnitude a is increasing, the AEP L_6 moves towards the primaries and L_7 moves towards the ξ-axis away from the primaries. Also, we have found the AEPs $L_{6,7}$ which are not symmetrical about the ξ-axis. From Figure 4, panel (c), we have observed that when the magnitude $a = 0.00015$ and α is increasing, the AEPs $L_{6,7}$ move towards the primaries. It is noticed that the AEPs $L_{6,7}$ are symmetrical about the ξ-axis. Further, from Figure 4, panel (d), we have observed that when the magnitude $a = 0.00015$ and α is increasing, the AEPs $L_{6,7}$ move towards the primaries. Also, we have found that the AEPs $L_{6,7}$ are not symmetrical about the ξ-axis. In addition, the numerical values of these out-of-plane AEPs are shown in Tables 5 ,6, 7, and 8 for few values of the parameters.

4. Stability of the artificial equilibrium points

In the present section, we shall discuss the linear stability of the AEPs with variable mass. Adopting the procedure of Mittal et al. (2016), we investigate the linear stability of the AEPs. Let u, v and w be the small displacements from the initial position of an AEP (ξ_0, η_0, ζ_0). Thus, the position of an AEP (ξ_0, η_0, ζ_0) can be expressed as $\xi = \xi_0 + u$, $\eta = \eta_0 + v$, $\zeta = \zeta_0 + w$, $(u,\ v,\ w << 1)$. Substituting all above displacements into Equestions (4), the linearized equations corresponding to Equestions (4) are given by:

$$\left.\begin{aligned} \ddot{u} - 2\dot{v} + (\Omega^*_{\xi\xi})_0\, u + (\Omega^*_{\xi\eta})_0\, v + (\Omega^*_{\xi\zeta})_0\, w = 0, \\ \ddot{v} + 2\dot{u} + (\Omega^*_{\eta\xi})_0\, u + (\Omega^*_{\eta\eta})_0\, v + (\Omega^*_{\eta\zeta})_0\, w = 0, \\ \ddot{w} + (\Omega^*_{\zeta\xi})_0\, u + (\Omega^*_{\zeta\eta})_0\, v + (\Omega^*_{\zeta\zeta})_0\, w = 0, \end{aligned}\right\} \tag{8}$$

where the subscript '0' in Equations (8) indicates that the values are to be calculated at the AEP $(\xi_0,\, \eta_0,\, \zeta_0)$ under consideration. Here, $\Omega^*_{\xi\xi},\, \Omega^*_{\eta\eta},\, \Omega^*_{\zeta\zeta},\, \Omega^*_{\xi\eta},\, \Omega^*_{\xi\zeta}$ and $\Omega^*_{\eta\zeta}$ are given by:

$$\begin{aligned}
\Omega^*_{\xi\xi} &= -\left(1+\frac{\alpha^2}{4}\right)+\gamma^{3/2}\left(\frac{1-\mu}{\rho_1^3}+\frac{\mu}{\rho_2^3}\right)\\
&\quad -3\gamma^{3/2}\left(\frac{(1-\mu)(\xi+\mu\sqrt{\gamma})^2}{\rho_1^5}+\frac{\mu\,(\xi+(-1+\mu)\sqrt{\gamma})^2}{\rho_2^5}\right),\\
\Omega^*_{\eta\eta} &= -\left(1+\frac{\alpha^2}{4}\right)-3\gamma^{3/2}\left(\frac{(1-\mu)\,\eta^2}{\rho_1^5}+\frac{\mu\eta^2}{\rho_2^5}\right)+\gamma^{3/2}\left(\frac{1-\mu}{\rho_1^3}+\frac{\mu}{\rho_2^3}\right),\\
\Omega^*_{\zeta\zeta} &= -\frac{\alpha^2}{4}-3\gamma^{3/2}\left(\frac{(1-\mu)\zeta^2}{\rho_1^5}+\frac{\mu\zeta^2}{\rho_2^5}\right)+\gamma^{3/2}\left(\frac{1-\mu}{\rho_1^3}+\frac{\mu}{\rho_2^3}\right),\\
\Omega^*_{\xi\eta} &= \Omega^*_{\eta\xi} = -3\gamma^{3/2}\left(\frac{(1-\mu)(\xi+\mu\sqrt{\gamma})\,\eta}{\rho_1^5}+\mu\frac{(\xi+(-1+\mu)\sqrt{\gamma})\,\eta}{\rho_2^5}\right),\\
\Omega^*_{\xi\zeta} &= \Omega^*_{\zeta\xi} = -3\gamma^{3/2}\left(\frac{(1-\mu)\,(\xi+\mu\sqrt{\gamma})\,\zeta}{\rho_1^5}+\frac{\mu\,(\xi+(-1+\mu)\sqrt{\gamma})\,\zeta}{\rho_2^5}\right),\\
\Omega^*_{\eta\zeta} &= \Omega^*_{\zeta\eta} = -3\gamma^{3/2}\left(\frac{(1-\mu)\,\eta\,\zeta}{\rho_1^5}+\frac{\mu\,\eta\,\zeta}{\rho_2^5}\right).
\end{aligned}$$

When $\alpha = 0$, then our problem with variable mass is similar to problem of constant mass. For $\alpha > 0$, the positions of the primaries vary with time and their distances to the AEP $(\xi_0,\, \eta_0,\, \zeta_0)$ decrease with time. So, the linear stability of the AEPs cannot be investigated by the method used in the case of constant mass. The space-time inverse transformations $(x = \gamma^{-1/2}\,\xi, y = \gamma^{-1/2}\,\eta$ and $z = \gamma^{-1/2}\,\zeta)$ of Meshcherskii (1949) have been used. The positions of the primaries are fixed so that their distances to the AEPs are invariable. We can write Equestions (8) in phase space by taking $\dot{u} = u_1, \dot{v} = v_1, \dot{w} = w_1$, as

$$\left.\begin{aligned}
\dot{u_1} - 2v_1 + (\Omega^*_{\xi\xi})_0\,u + (\Omega^*_{\xi\eta})_0\,v + (\Omega^*_{\xi\zeta})_0\,w = 0,\\
\dot{v_1} + 2u_1 + (\Omega^*_{\eta\xi})_0\,u + (\Omega^*_{\eta\eta})_0\,v + (\Omega^*_{\eta\zeta})_0\,w = 0,\\
\dot{w_1} + (\Omega^*_{\zeta\xi})_0\,u + (\Omega^*_{\zeta\eta})_0\,v + (\Omega^*_{\zeta\zeta})_0\,w = 0.
\end{aligned}\right\} \tag{9}$$

Introducing Meshcherskii (1949) inverse transformations, and considering

$$x' = \gamma^{-1/2}u, y' = \gamma^{-1/2}v, z' = \gamma^{-1/2}w, u' = \gamma^{-1/2}u_1, v' = \gamma^{-1/2}v_1, w' = \gamma^{-1/2}w_1,$$

the Equestions (9) can be written in the matrix form as follows:

$$\begin{pmatrix}
\frac{dx'}{dt}\\ \frac{dy'}{dt}\\ \frac{dz'}{dt}\\ \frac{du'}{dt}\\ \frac{dv'}{dt}\\ \frac{dw'}{dt}
\end{pmatrix} =
\begin{pmatrix}
\frac{\alpha}{2} & 0 & 0 & 1 & 0 & 0\\
0 & \frac{\alpha}{2} & 0 & 0 & 1 & 0\\
0 & 0 & \frac{\alpha}{2} & 0 & 0 & 1\\
-(\Omega^*_{\xi\xi})_0 & -(\Omega^*_{\xi\eta})_0 & -(\Omega^*_{\xi\zeta})_0 & \frac{\alpha}{2} & 2 & 0\\
-(\Omega^*_{\eta\xi})_0 & -(\Omega^*_{\eta\eta})_0 & -(\Omega^*_{\eta\zeta})_0 & -2 & \frac{\alpha}{2} & 0\\
-(\Omega^*_{\zeta\xi})_0 & -(\Omega^*_{\zeta\eta})_0 & -(\Omega^*_{\zeta\zeta})_0 & 0 & 0 & \frac{\alpha}{2}
\end{pmatrix}
\begin{pmatrix}
x'\\ y'\\ z'\\ u'\\ v'\\ w'
\end{pmatrix}. \tag{10}$$

The linear stability analysis of each AEP can be found through the characteristic roots of the coefficient matrix of Equestion (10) numerically. The characteristic equation corresponding to

linearized equations of motion is

$$\left.\begin{aligned}\lambda^6 - 3\alpha\lambda^5 + \left(\frac{15}{4}\alpha^2 + P\right)\lambda^4 - \left(\frac{5}{2}\alpha^3 + 2\,P\alpha\right)\lambda^3 + \left(\frac{15}{16}\alpha^4 + \frac{3}{2}P\alpha^2 + Q\right)\lambda^2 \\ - \left(\frac{3}{16}\alpha^5 + \frac{1}{2}P\alpha^3 + Q\alpha\right)\lambda + \left(\frac{1}{64}\alpha^6 + \frac{1}{16}P\alpha^4 + \frac{1}{4}Q\alpha^2 + R\right) = 0\,,\end{aligned}\right\} \tag{11}$$

where

$$\begin{aligned}P &= (\Omega^*_{\xi\xi})_0 + (\Omega^*_{\eta\eta})_0 + (\Omega^*_{\zeta\zeta})_0 + 4,\\ Q &= (\Omega^*_{\xi\xi})_0\,(\Omega^*_{\eta\eta})_0 + (\Omega^*_{\xi\xi})_0\,(\Omega^*_{\zeta\zeta})_0 + (\Omega^*_{\eta\eta})_0\,(\Omega^*_{\zeta\zeta})_0\\ &\quad -(\Omega^*_{\xi\eta})_0^2 - (\Omega^*_{\xi\zeta})_0^2 - (\Omega^*_{\eta\zeta})_0^2 + 4\,(\Omega^*_{\zeta\zeta})_0,\\ R &= (\Omega^*_{\xi\xi})_0\,(\Omega^*_{\eta\eta})_0\,(\Omega^*_{\zeta\zeta})_0 + 2(\Omega^*_{\xi\eta})_0\,(\Omega^*_{\xi\zeta})_0\,(\Omega^*_{\eta\zeta})_0 - (\Omega^*_{\xi\eta})_0^2\,(\Omega^*_{\zeta\zeta})_0\\ &\quad -(\Omega^*_{\xi\zeta})_0^2\,(\Omega^*_{\eta\eta})_0 - (\Omega^*_{\eta\zeta})_0^2\,(\Omega^*_{\xi\xi})_0.\end{aligned}$$

To determine the linear stability of the system of AEPs, we must find the roots of Equestion (11). The roots of Equestion (11) have been calculated at various AEPs for $\mu = 0.019$ in the range $0 < \gamma < 1$, $0 < \alpha \leq 2.2$. As in Mittal et al. (2016), we have observed that there always exists at least one positive real eigenvalue at each AEP. Hence, we have concluded that all the AEPs are unstable for $\alpha > 0$.

5. Zero velocity curves

The zero velocity curves (ZVCs) in the circular restricted three-body problem have been investigated by many authors for different values of Jacobian constant C. We have investigated these ZVCs by taking the numerical value of Jacobian constant C and setting the velocity terms in the Jacobian integral to zero. We have adopted the procedure of Abouelmagd and Mostafa (2015), the conditions of motion can be read as

$$\Omega^*(\gamma) \geq C(\gamma) \text{ for } \tfrac{\partial\Omega^*}{\partial\gamma} \geq 0,\ \Omega^*(\gamma_0) \geq C(\gamma_0) \text{ for } \tfrac{\partial\Omega^*}{\partial\gamma} \leq 0.$$

The Jacobian integral of the equations of motion with continuous low-thrust is defined as:

$$C(\gamma_0) = \Omega^*\left(\gamma, \xi_0, \eta_0, \zeta_0\right) + \frac{1}{2}(\dot{\xi}^2 + \dot{\eta}^2 + \dot{\zeta}^2). \tag{12}$$

The subscripts '0' indicate the initial value of the corresponding variables. We have drawn the ZVCs from Equestion (12) by taking $\dot{\xi} = \dot{\eta} = \dot{\zeta} = 0$. The white domains correspond to the Hill's region, and cyan color indicates the forbidden regions, while the thick black lines show the ZVCs. In these ZVCs, the black dots indicate the positions of the AEPs, while the blue dots indicate the positions of two primaries.

In Figure 5, we have plotted the ZVCs from Equestion (12) for the fixed values of $C = -0.163047$, $\mu = 0.019$, $\alpha = 0.2$, $\gamma = 0.1$, $\theta = 0$, $\phi = 0$ and for different values of the magnitude a of continuous low-thrust acceleration. Panel (a) shows the ZVC for magnitude $a = 0.00015$ and indicates that

there exist circular land (white domains) around the primaries and the spacecraft trapped in these regions, where the motion is possible and the circular strip (cyan color) shows the forbidden region in which the motion of spacecraft is not possible. Thus, the spacecraft can move around both the primaries and can not move from one primary to other primary. In panel (b), we have increased the value of magnitude $a = 0.00043$ and observed that the inner circular boundary breaks at L_1. Therefore, the spacecraft can move freely from one primary to other primary, while the spacecraft is restricted to move outside the outer circular boundary.

Figure 5, panel (c) is drawn for $a = 0.0028$. We have observed that the spacecraft can freely move from one primary to other primary. For $a = 0.00365$ in panel (d), there exist a limiting situation and a cusp at L_3, it is observed that the spacecraft can freely move in whole white domain. In panel (e), we have seen two branches of zero velocity curve containing forbidden regions (cyan color) for $a = 0.0041$. The AEP L_4 lies in the first branch and L_5 in other branch. In the last, panel (f) is drawn for $a = 0.00425$; there exist forbidden regions around L_4 and L_5 in tadpole shaped form and the spacecraft can move from one primary to other primary.

The ZVCs in Figure 6(a) have drawn for $C_1 = -0.163047$, $C_2 = -0.153547$, $C_3 = -0.152047$, $C_4 = -0.151047$ $C_5 = -0.150447$, $C_6 = -0.150097$ and for fixed values of $\mu = 0.019$, $\alpha = 0.2$, $\gamma = 0.1$, $\theta = 0$, $\phi = 0$ and for magnitude $a = 0.00015$. We have observed that the regions of motion increase for the increasing values of Jacobian constant C. In Figure 6(b), we have determined the ZVCs for fixed values of mass parameter $\mu = 0.019$, $\gamma = 0.1$, $C = -0.163047$, $\theta = 0$, $\phi = 0$, $a = 0.00015$ and for different values of $\alpha = 0.2, 0.75, 0.995, 1.055, 1.08, 1.095$. The bounded curves show the forbidden regions where the motion of the spacecraft is not possible, while the motion of the spacecraft is possible outside the bounded curve.

The ZVCs in Figure 7 have drawn for fixed values of $C = -0.164944$, $\mu = 0.019$, $\alpha = 0.2$, $\gamma = 0.1$, $\theta = 0$, $\phi = \pi/2$ and for different values of the magnitude a of low-thrust acceleration $\boldsymbol{a}$ in the $\xi\eta$-plane. The cyan color shows the forbidden region where the motion of spacecraft is not possible but the spacecraft can freely move in white domain. It has been observed that the regions of motion increase for the increasing values of magnitude a of low-thrust acceleration $\boldsymbol{a}$.

In Figure 8, we have drawn the out of plane zero velocity curves for $C = -0.1878643$, $\mu = 0.019$, $\alpha = 0.2$, $\gamma = 0.1$, $\theta = \pi/2$, $\phi = 0$ and for different values of magnitude $a = 0.0095, 0.0145, 0.0160, 0.0174$ in the $\xi\zeta$-plane. The black dots indicate the positions of the out-of-plane artificial equilibrium points and blue dots indicate the positions of the primaries. The cyan color in Figure 8 (a,b,c,d) indicate the forbidden regions in which the motion of the spacecraft is not allowed. From Figure 8, we have observed that the regions of motion expand for the increasing values of the magnitude a of low-thrust acceleration $\boldsymbol{a}$.

6. Discussion

In this paper, we have incorporated the new parameter of low-thrust acceleration in the restricted three-body problem with the effect of variable mass. The idea of introducing the new parameter

of low-thrust acceleration in the R3BP with the effect of variable mass is a new study. We have investigated the existence and stability of the AEPs in the low-thrust R3BP with the effect of variable mass when both the primaries are point masses. The important findings of our study follow.

It is found that there exist three collinear and two non-collinear AEPs if $\theta = 0,\ \phi = 0$ for increasing values of magnitude a and their numerical values are shown in Tables 1, 3. Further, from Tables 2 and 4, we have observed that there exist only non-collinear AEPs when $\theta = 0,\ \phi = \pi/2$ for increasing values of magnitude a. We have obtained two out-of-plane AEPs which are displayed in Tables 5, 6, 7, and 8. We have observed that the variable mass parameter α affected the positions of the AEPs. In this model of the low-thrust restricted three-body problem with variable mass all the AEPs are new positions of the equilibrium points. Further, we have determined the linear stability of the AEPs. It has been observed that all the AEPs are unstable for $\alpha > 0$ and for all values of the low-thrust acceleration. Our results are different from Morimoto et al. (2007), because they have studied the model of low-thrust restricted three-body problem with constant mass, whereas we have studied the model of low-thrust restricted three-body problem with variable mass. Our model of the restricted three-body problem with variable mass is different from the model of Zhang et al. (2012) due to the presence of continuous low-thrust acceleration $\boldsymbol{a}$. Therefore, our results are different from Zhang et al. (2012), in some aspects given below. (1) They have studied the photogravitational restricted three-body problem with variable mass, whereas we have studied the low-thrust restricted three-body problem with variable mass. (2) They have obtained only two non-collinear triangular equilibrium points whereas we have obtained three collinear and two non-collinear AEPs in the $\xi\eta$-plane if $\theta = 0,\ \phi = 0$ and the magnitude a is increasing but we have obtained five non-collinear AEPs $\xi\eta$-plane if $\theta = 0,\ \phi = \pi/2$ and the magnitude a is increasing.

Finally, we have drawn the zero velocity curves to determine the possible regions of motion in which the spacecraft is free to move. From Figure (5), we have observed that for increasing values of magnitude a, the possible regions of motion increase in which the spacecraft can freely move from one place to other place. From the results in Figure 6 (a), we conclude that for different values of Jacobian constant C, we have different trapped areas in which the spacecraft can move. Further, from Figure 6 (b), we have observed that the regions of motion increase for the increasing values of $\alpha\,(0 < \alpha \leq 2.2)$ and for fixed values of remaining parameters.

Furthermore, from Figures 7 and 8, it has been observed that the regions of motion increase for the increasing values of magnitude a of low-thrust acceleration $\boldsymbol{a}$. In this model of the low-thrust restricted three-body problem with variable mass, the vital effect of the low-thrust acceleration $\boldsymbol{a}$ is observed on the regions of motion. The AEPs do not depend only on the magnitude but also on the directions of the continuous low-thrust acceleration $\boldsymbol{a}$. Both the angle parameters θ and ϕ of the continuous low-thrust acceleration $\boldsymbol{a}$ have the physical significance. We can find the arbitrary positions of the spacecraft in the whole space with a choice of the magnitude and the directions θ and ϕ of the low-thrust acceleration $\boldsymbol{a}$. We can take the values of space angles θ and ϕ in the range $0 \leq \theta, \phi \leq 2\pi$. This paper is applicable for few solar system bodies which hover around the other.

7. Conclusion

In this paper, we have studied the existence and the stability of the artificial equilibrium points in low-thrust restricted three-body problem under the effect of variable mass. First, we have derived the equations of motion of the spacecraft after using the space-time transformations of Meshcherskii. Second, we have investigated the artificial equilibrium points under the effect of control acceleration. Further, we have studied the linear stability of the artificial equilibrium points under the effect of variable mass. We have observed that all the artificial equilibrium points are unstable for all the values of the related parameters. Finally, we have plotted the zero velocity curves for the in-plane and out-of-plane artificial equilibrium points. We have observed that the regions of motion increase for the increasing values of the magnitude of control acceleration in which the spacecraft can move in all the places without any barrier. Also, it is observed that the magnitude of the control acceleration has significant impact on the regions of motion.

Acknowledgment:

Authors are thankful to the Centre of Fundamental Research in Space Dynamics and Celestial Mechanics (CFRSC), New Delhi, India for giving some necessary study materials and other supporting items which are required for the present research work.

REFERENCES

Abouelmagd, E. I. and Mostafa, A. (2015). Out of plane equilibrium points locations and the forbidden movement regions in the restricted three-body problem with variable mass, Astrophys. Space Sci., Vol. 346, No. 48. doi:10.1007/s10509-015-2294-7

Aliasi, G., Mengali, G. and Quarta, A. (2011). Artificial equilibrium points for a generalized sail in the circular restricted three-body problem, Celest. Mech. Dyn. Astron., Vol. 110, pp. 343-368.

Aliasi, G., Mengali, G. and Quarta, A. (2012). Artificial equilibrium points for a generalized sail in the elliptic restricted three-body problem, Celest. Mech. Dyn. Astron., Vol. 114, pp. 181-200. doi:10.1007/s10569-012-9425-z

Baig, S. and McInnes, C. R. (2008). Artificial three-body equilibria for hybrid low-thrust propulsion, J. Guid. Control Dyn., Vol. 31, No. 6, pp. 1644-1655.

Bombardelli, C. and Pelaez, J. (2011). On the stability of artificial equilibrium points in the circular restricted three-body problem, Celest. Mech. Dyn. Astron., Vol. 109, No. 1, pp. 13-26. doi:10.1007/s10569-010-9317

Broschart, S.B. and Scheeres, D. J. (2005). Control of hovering spacecraft near small bodies: Application to Asteroid 25143 Itokwa, J. Guid. Control Dyn., Vol. 28, No. 2, pp. 343-354.

Bu, S., Li, S. and Yang, H. (2017). Artificial equilibrium points in binary asteroid systems with

continuous low-thrust, Astrophys. Space Sci., Vol. 362, No. 137. doi:10.1007/s10509-017-31197-7

Dusek, H. M. (1966). Motion in the vicinity of libration points of a generalized restricted three-body model, Prog. Astronaut. Rocket., Vol. 17, pp. 37-54.

Farquhar, R. W. (1967). Lunar communications with libration-point satellites, Spacecraft and Rockets, Vol. 4, No. 10, pp. 1383-1384.

Jeans, J. H. (1928). *Astronomy and Cosmology*, Cambridge University Press, Cambridge.

Lu, T. W. (1990). Analysis on the stability of triangular points in the restricted problem of three-bodies with variable mass, Publ. Purple Mt. Obs., Vol. 9, No. 4, pp. 290-296.

Meshcherskii, I. V. (1949). Studies on the mechanics of bodies of variable mass, GITTL, Moscow.

Meshcherskii, I. V. (1952). Work on the mechanics of bodies of variable mass, GITTL, Moscow.

Mittal, A., Aggarwal, R., Suraj, M. S. and Arora, M. (2018a). On the photo-gravitational restricted four-body problem with variable mass, Astrophys. Space Sci., Vol. 363, No. 109. doi:10.1007/s10509-018-3321-2.

Mittal, A., Aggarwal, R., Suraj, M. S. and Bisht, V. S. (2016). Stability of libration points in the restricted four-body problem with variable mass, Astrophys. Space Sci., Vol. 361, No. 329. doi:10.1007/s10509-016-2901-2.

Mittal, A., Arora, M., Suraj, M. S. and Aggarwal, R. (2018b). The basins of convergence in the planar restricted four-body problem with variable mass, Appl. Appl. Math., Vol. 13, No. 2, pp. 1230-1247. doi:10.1007/s10509-018-3321-2

Mittal. A. and Pal. K. (2018). Artificial equilibrium points in the low-thrust restricted three-body problem when both the primaries are oblate spheroids, Int. J. Astron. Astrophys., Vol. 8, pp. 406-424.

Morimoto, M. Y., Yamakawa, H. and Uesugi, K. (2007). Artificial equilibrium points in the low-thrust restricted three-body problem, J. Guid. Control Dyn., Vol. 30, No. 5, pp. 1563-1567.

Ranjana, K. and Kumar, V. (2013). On the artificial equilibrium points in a generalized restricted problem of three-bodies, Int. J. Astron. Astrophys., Vol. 3, No. 4, pp. 508-516.

Shrivastava, A. K. and Ishwar, B. (1983). Equations of motion in the restricted problem of three bodies with variable mass, Celest. Mech., Vol. 30, pp. 323-328.

Singh, J. (2003). Photogravitational restricted three-body problem with variable mass, Indian J. Pure Appl. Math., Vol. 34, No. 2, pp. 335-341.

Singh, J. (2008). Non-linear stability of equilibrium points in the restricted three-body problem with variable mass, Astrophys. Space Sci., Vol. 314, pp. 281-289.

Singh, J. (2009). Effect of perturbations on the non-linear stability of triangular points in the restricted three-body problem with variable mass, Astrophys. Space Sci., Vol. 321, pp. 127-135.

Singh, J. (2011). Non-linear stability in the restricted three-body problem with oblateness and variable mass, Astrophys. Space Sci., Vol. 333, pp. 61-69.

Singh, J. and Ishwar, B. (1984). Effect of perturbations on the location of equilibrium points in the restricted problem of three bodies with variable mass, Celest. Mech., Vol. 32, No. 4, pp. 297-305.

Singh, J. and Ishwar, B. (1985). Effect of perturbations on the stability of triangular points in the restricted problem of three bodies with variable mass, Celest. Mech., Vol. 35, pp. 201-207.

Singh, J. and Leke. (2010). Stability of photogravitational restricted three-body problem with

variable mass, Astrophys. Space Sci., Vol. 362, No. 2, pp. 305-314.

Suraj, M. S., Mittal, A. and Aggarwal, R. (2018a). Revealing the existence and stability of equilibrium points in the circular autonomous restricted four-body problem with variable mass, New Astronomy. https://doi.org/10.1016/j.newast.2018.10.003

Suraj, M. S., Mittal, A., Charanpreet, K. and Aggarwal, R. (2018b). On the existence of libration points in the spatial collinear restricted four-body problem within frame of repulsive Manev potential and variable mass, Chaos, Solitons and Fractals, Vol. 117, pp. 94-104.

Suraj, M. S., Abouelmagd, E. I., Mittal, A. and Aggarwal, R. (2019). The analysis of restricted five-body problem within frame of variable mass, New Astronomy, Vol. 7 0, pp. 12-21.

Suraj, M. S., Mittal, A., Charanpreet, K. and Aggarwal, R. (2020a). Analysis of Copenhagen problem with a repulsive quasi-homogeneous Manev-type potential within the frame of variable mass, Astron. Nachr., pp. 1-14. https://doi.org/10.1002/asna.202013640

Suraj, M. S., Mittal, A. and Pal, K. (2020b). Stability of the artificial equilibrium points in the low-thrust restricted three-body problem when the bigger primary is a source of radiation, Nonlinear Dynamics and Systems Theory, Vol. 20, No. 3, pp. 333-344.

Suraj, M. S., Mittal, A., Pal, K. and Mittal, D. (2020c). Stability of the artificial equilibrium points in the low-thrust restricted three-body problem when the smaller primary is an oblate spheroid, Nonlinear Dynamics and Systems Theory, Vol. 20, No. 4, pp. 439-450.

Szebehely, V. (1967). *Theory of Orbits, the Restricted Problem of Three-bodies*, Academic Press, New York.

Yang, H.W., Zeng, X.Y. and Baoyin, H. (2015). Feasible region and stability analysis for hovering around elongated asteroids with low-thrust, Res. Astron. Astrophys., Vol. 15, No. 9, pp. 1571-1585. doi:10.1088/1674-4527/15/9/013.

Zhang, M.J., Zhao, C.Y. and Xiong, Y.Q. (2012). On the triangular libration points in photogravitational restricted three-body problem with variable mass, Astrophys. Space Sci., Vol. 337, pp. 107-113.

Appendix

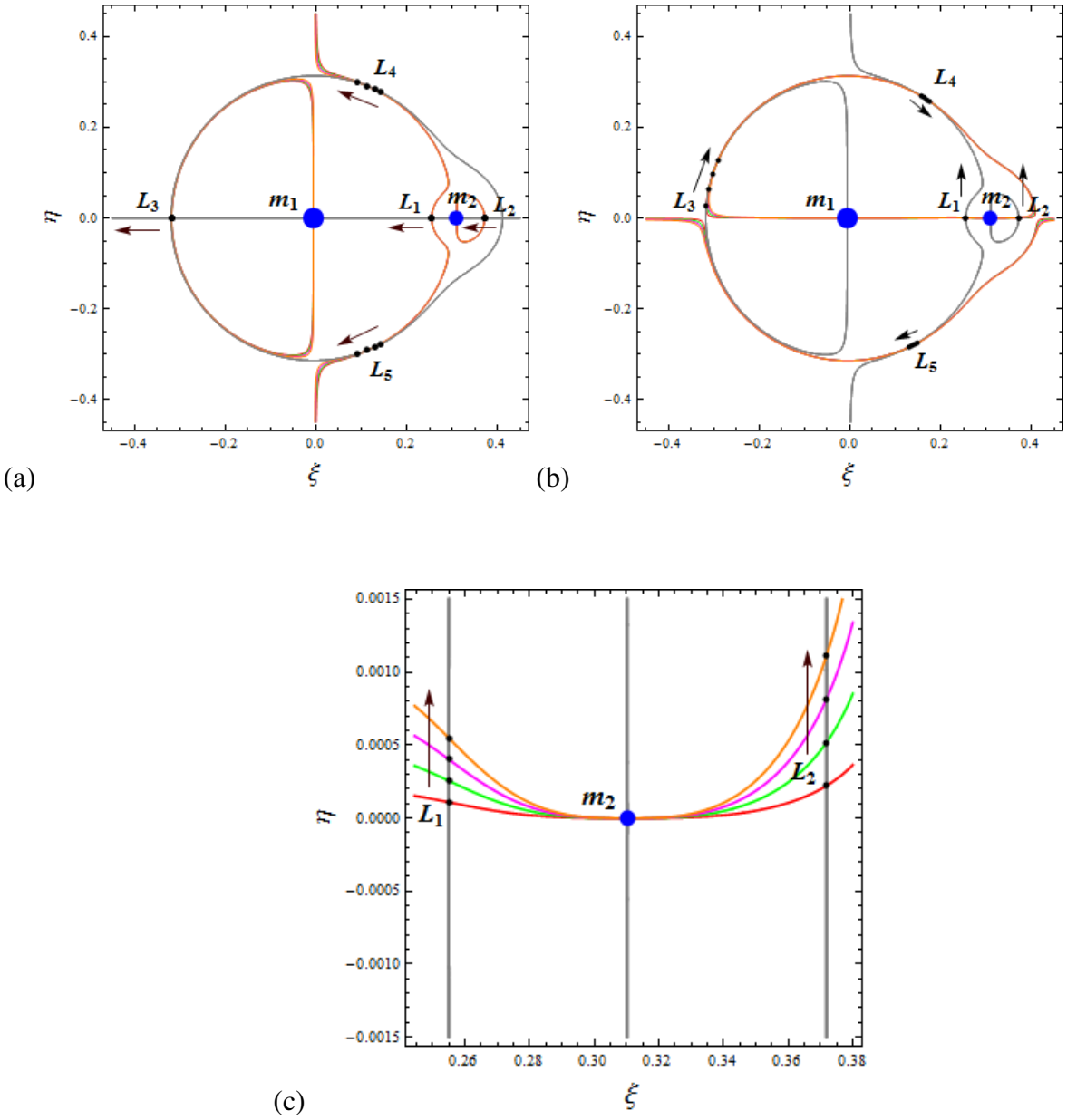

Figure 2. The locations of five AEPs in the low-thrust R3BP with variable mass for $\mu = 0.019$, $\alpha = 0.2$, $\gamma = 0.1$, (a) for $\theta = 0$, $\phi = 0$ and $a = 0.00015, 0.00035, 0.00055, 0.00075$, (b) for $\theta = 0$, $\phi = \pi/2$ and $a = 0.00015$, 0.00035, 0.00055, and 0.00075, and panel (c) shows the zoomed part of panel (b) near the primary m_2

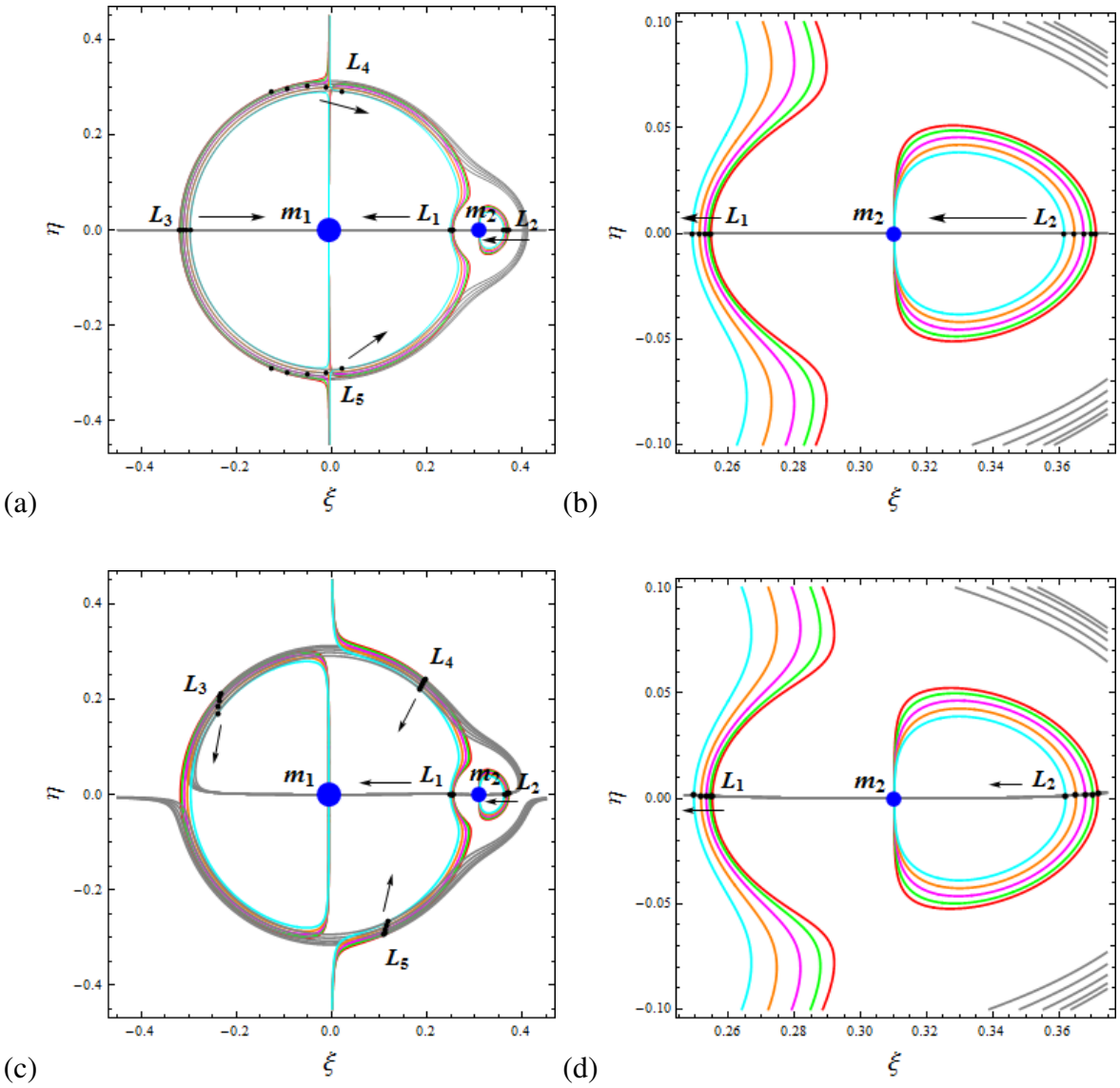

Figure 3. The locations of five AEPs in the low-thrust R3BP with variable mass for $\mu = 0.019$, $\gamma = 0.1$, (a) for $\theta = 0$, $\phi = 0$, $a = 0.0015$ and $\alpha = 0.2, 0.4, 0.6, 0.8, 1$, (b) is the zoomed part of panel (a) near the primary m_2, (c) for $\theta = 0$, $\phi = \pi/2$, $a = 0.0015$ and $\alpha = 0.2, 0.4, 0.6, 0.8, 1$ and panel (d) shows the zoomed part of panel (c) near the primary m_2

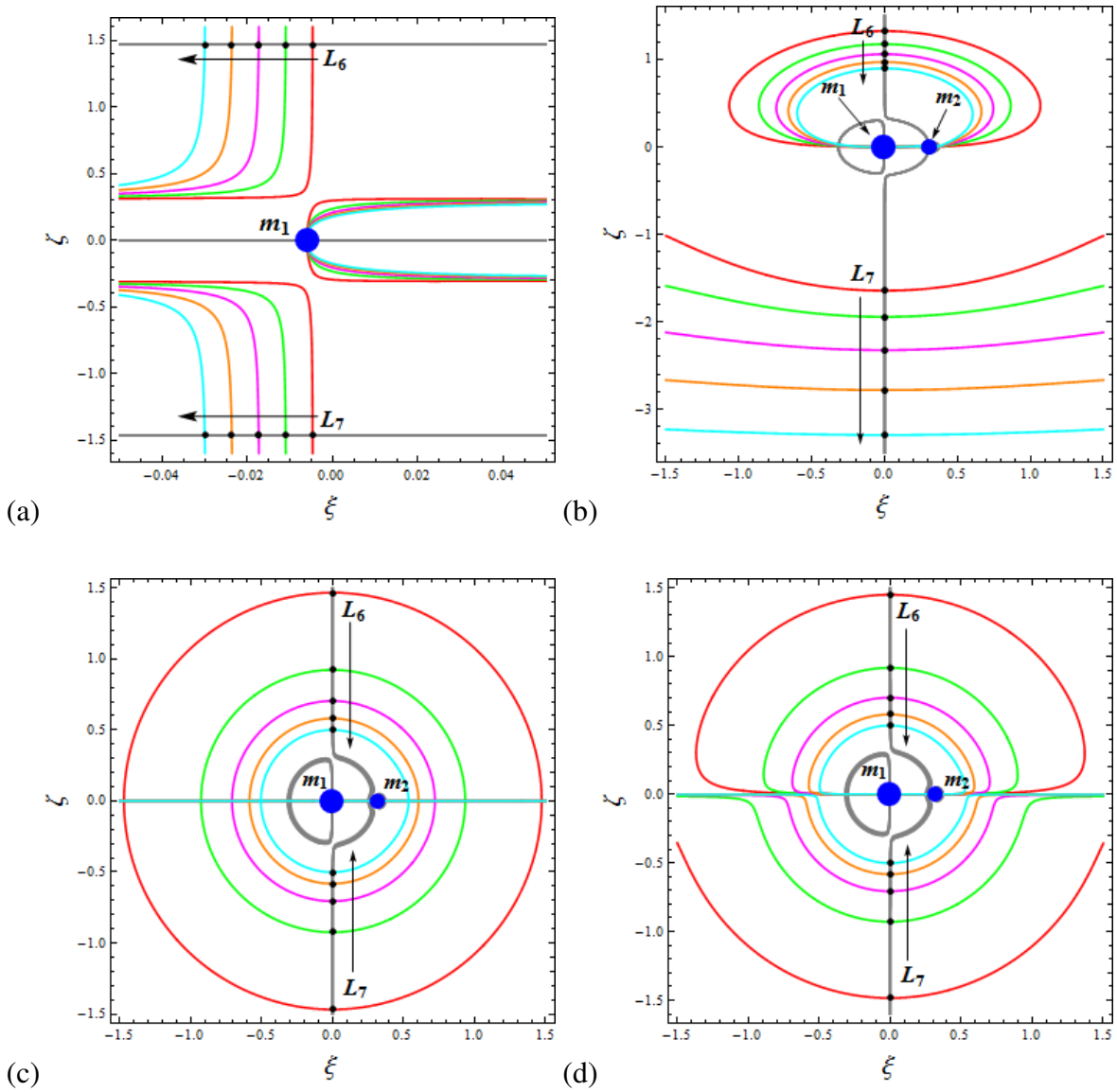

Figure 4. The locations of out-of-plane AEPs $L_{6,7}$ in the low-thrust R3BP with variable mass for $\mu = 0.019$, $\alpha = 0.2$, $\gamma = 0.1$, (a) $\theta = 0$, $\phi = 0$ and $a = 0.0015, 0.0035, 0.0055, 0.0075$ and 0.0095, (b) $\theta = \pi/2$, $\phi = 0$ and $a = 0.0015, 0.0035, 0.0055, 0.0075, 0.0095$ and $\alpha = 0.2$, (c) for $\theta = 0$, $\phi = 0$, $a = 0.00015$ and $\alpha = 0.2, 0.4, 0.6, 0.8, 1$, (d) for $\theta = \pi/2$, $\phi = 0$, $a = 0.00015$ and $\alpha = 0.2, 0.4, 0.6, 0.8, 1$

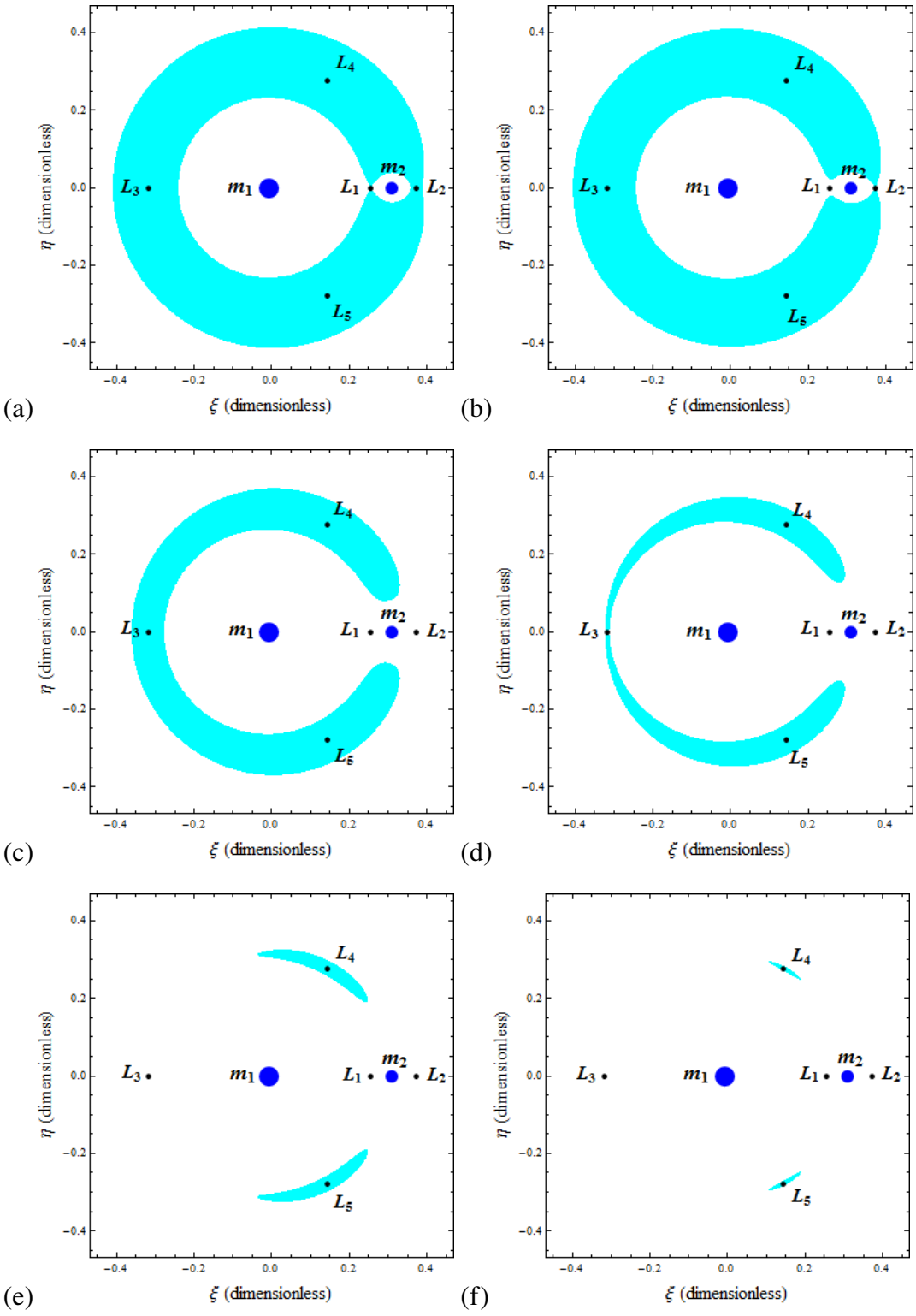

Figure 5. The ZVCs in the low-thrust R3BP for $\mu = 0.019$, $\alpha = 0.2$, $\gamma = 0.1$, $C = -0.163047$ and $\theta = 0$, $\phi = 0$, (a) for $a = 0.00015$, (b): $a = 0.00043$, (c): $a = 0.0028$, (d): $a = 0.00365$, (e): $a = 0.0041$, (f): $a = 0.00425$

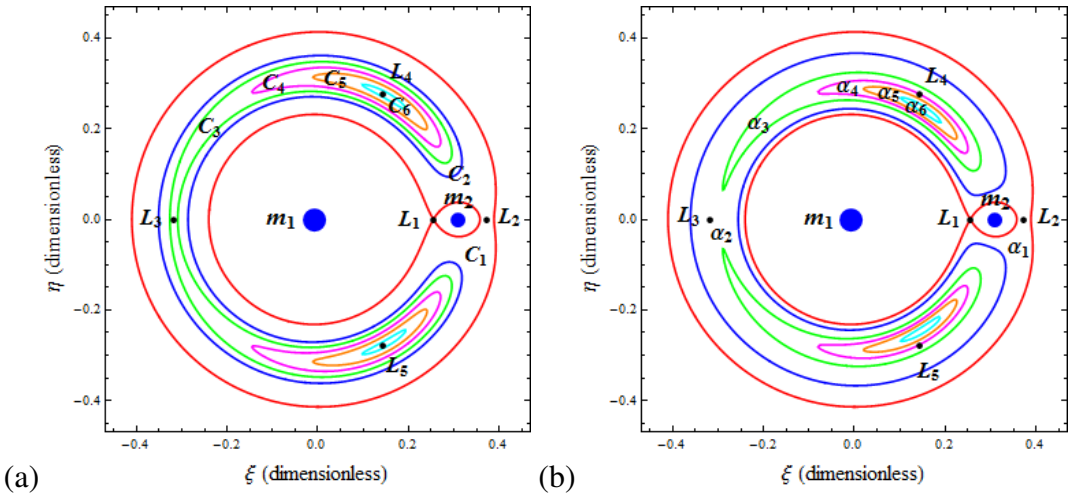

Figure 6. The ZVCs in the low-thrust R3BP with variable mass for $\mu = 0.019$, $\gamma = 0.1$, $\theta = 0$, $\phi = 0$ and $a = 0.00015$, (a) for different values of the Jacobian constant C with $\alpha = 0.2$, (b) for different values of α and $C = -0.163047$

Table 1. The AEPs in $\xi\eta$-plane when a is increasing

$\mu = 0.019$ $\alpha = 0.2, \gamma = 0.1$ $\theta = 0, \phi = 0$			
a	L_1	L_2	L_3
0.00015	(0.255027, 0)	(0.371769, 0)	(-0.317842, 0)
0.00035	(0.254972, 0)	(0.371684, 0)	(-0.318049, 0)
0.00055	(0.254917, 0)	(0.371597, 0)	(-0.318256, 0)
0.00075	(0.254860, 0)	(0.371514, 0)	(-0.318463, 0)
$L_{4,5}$			
(0.143189, $\pm$ 0.277451)			
(0.129170, $\pm$ 0.284310)			
(0.111866, $\pm$ 0.291682)			
(0.089813, $\pm$ 0.299431)			

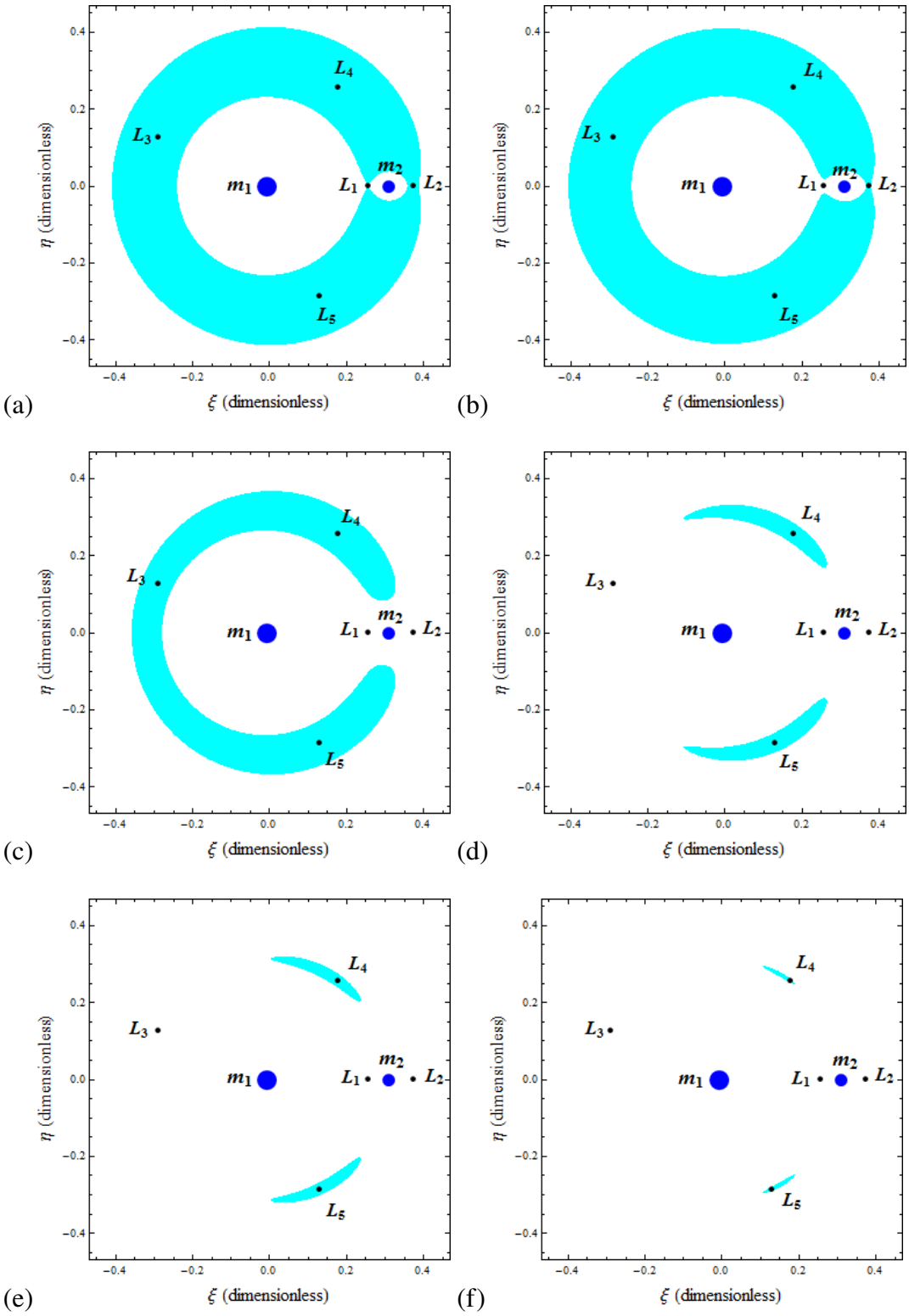

Figure 7. The ZVCs in the low-thrust R3BP with variable mass. For $\mu = 0.019$, $\alpha = 0.2$, $\gamma = 0.1$, $\theta = 0$, $\phi = \pi/2$ and (a) for $a = 0.00075$, (b): $a = 0.00099$, (c): $a = 0.0035$, (d): $a = 0.0046$, (e): $a = 0.00475$, (f): $a = 0.00485$

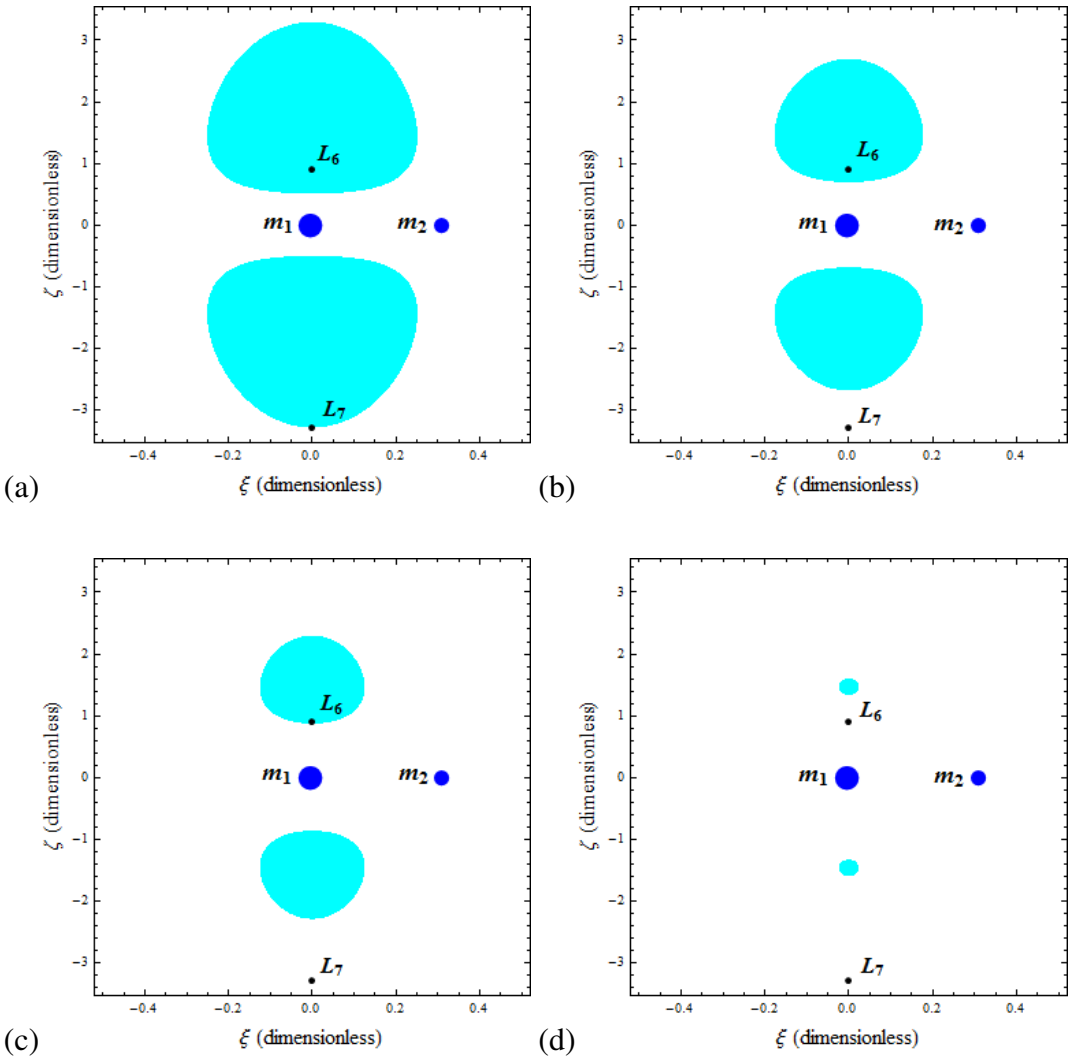

Figure 8. Out-of-plane ZVCs in the low-thrust R3BP with variable mass. For $\mu = 0.019$, $\alpha = 0.2$, $\gamma = 0.1$, $\theta = \pi/2$, $\phi = 0$ and for different values of a. (a) for $a = 0.0095$, (b): $a = 0.0145$, (c): $a = 0.0160$, (d): $a = 0.0174$

Table 2. The AEPs in $\xi\eta$-plane when a is increasing

$\mu = 0.019$ $\alpha = 0.2, \gamma = 0.1$ $\theta = 0, \phi = \pi/2$		
a	L_1	L_2
0.00015	(0.255066, 0.000109939)	(0.371759, 0.000221298)
0.00035	(0.255066, 0.000256527)	(0.371832, 0.000518731)
0.00055	(0.255067, 0.000403118)	(0.371833, 0.000815135)
0.00075	(0.255068, 0.000549716)	(0.371834, 0.001111510)
L_3	L_4	L_5
(-0.316441, 0.0277905)	(0.156768, 0.269789)	(0.147466, -0.275398)
(-0.311049, 0.0638407)	(0.162979, 0.265806)	(0.141351, -0.278865)
(-0.301921, 0.0976463)	(0.169136, 0.261659)	(0.135362, -0.282102)
(-0.289895, 0.1283370)	(0.175187, 0.257381)	(0.129540, -0.285104)

Table 3. The AEPs in $\xi\eta$-plane when α is varying

$\mu = 0.019$ $\gamma = 0.1$ $\theta = 0, \phi = 0$ $a = 0.0015$				
α	L_1	L_2	L_3	$L_{4,5}$
0.2	(0.254660, 0)	(0.371190, 0)	(-0.319243, 0)	(-0.1255660, $\pm$ 0.289922)
0.4	(0.253992, 0)	(0.369744, 0)	(-0.316148, 0)	(-0.0932165, $\pm$ 0.298112)
0.6	(0.252857, 0)	(0.367518, 0)	(-0.311246, 0)	(-0.0523986, $\pm$ 0.302311)
0.8	(0.251225, 0)	(0.364741, 0)	(-0.304870, 0)	(-0.0124166, $\pm$ 0.299584)
1	(0.249072, 0)	(0.361639, 0)	(-0.297393, 0)	(0.0221290, $\pm$ 0.291015)

Table 4. The AEPs in $\xi\eta$-plane when α is varying

$\mu = 0.019$ $\gamma = 0.1$ $\theta = 0, \phi = \pi/2$ $a = 0.0015$		
α	L_1	L_2
0.2	(0.255075, 0.00109955)	(0.371791, 0.00222253)
0.4	(0.254414, 0.00113710)	(0.370314, 0.00205720)
0.6	(0.253292, 0.00120271)	(0.368040, 0.00182001)
0.8	(0.251681, 0.00130105)	(0.365202, 0.00155170)
1	(0.249544, 0.00143906)	(0.362040, 0.00128687)
L_3	L_4	L_5
(-0.234184, 0.211604)	(0.196243, 0.240752)	(0.109663, -0.294360)
(-0.235457, 0.205716)	(0.194633, 0.238121)	(0.110824, -0.290569)
(-0.237206, 0.196420)	(0.192186, 0.233865)	(0.112642, -0.284529)
(-0.238980, 0.184411)	(0.189184, 0.228165)	(0.114963, -0.276607)
(-0.240323, 0.170521)	(0.185913, 0.221248)	(0.117611, -0.267219)

Table 5. Out-of-plane AEPs in the $\xi\zeta$-plane when a is varying

$\mu = 0.019,\ \alpha = 0.2, \gamma = 0.1, \theta = 0, \phi = 0$	
a	$L_{6,7}$
0.0015	(-0.00473956, $\pm$1.46719)
0.0035	(-0.01106400, $\pm$1.46716)
0.0055	(-0.01738840, $\pm$1.46710)
0.0075	(-0.02371280, $\pm$1.46702)
0.0095	(-0.03003720, $\pm$1.46690)

Table 6. Out-of-plane AEPs in the $\xi\zeta$-plane when a is varying

$\mu = 0.019$ $\alpha = 0.2, \gamma = 0.1$ $\theta = \pi/2, \phi = 0$		
a	L_6	L_7
0.0015	(0.0000061884, 1.324780)	(0.0000021398000, -1.64367)
0.0035	(0.0000111039, 1.175900)	(0.0000009347770, -1.94345)
0.0055	(0.0000183250, 1.061410)	(0.0000003849490, -2.32430)
0.0075	(0.0000282504, 0.971311)	(0.0000001579850, -2.78057)
0.0095	(0.0000412352, 0.898769)	(0.0000000678393, -3.29530)

Table 7. Out-of-plane AEPs in the $\xi\zeta$-plane when α is varying

$\mu = 0.019, \gamma = 0.1$ $\theta = 0, \phi = 0$ $a = 0.00015$	
α	$L_{6,7}$
0.2	(-0.0004705850, $\pm$ 1.467200)
0.4	(-0.0004392500, $\pm$ 0.923769)
0.6	(-0.0003497940, $\pm$ 0.704575)
0.8	(-0.0001769330, $\pm$ 0.581308)
1	(0.0000977794, $\pm$ 0.500715)

Table 8. Out-of-plane AEPs in the $\xi\zeta$-plane when α is varying

$\mu = 0.019, \gamma = 0.1$ $\theta = \pi/2, \phi = 0$ $a = 0.00015$		
α	L_6	L_7
0.2	(0.00000394877, 1.451540)	(0.00000355093, -1.483190)
0.4	(0.00003573170, 0.919826)	(0.00003427130, -0.927745)
0.6	(0.00012575400, 0.702817)	(0.00012273200, -0.706340)
0.8	(0.00029922700, 0.580317)	(0.00029423900, -0.582299)
1	(0.00057459900, 0.500077)	(0.00056727500, -0.501347)